J Mater Sci (2011) 46:4162–4168
DOI 10.1007/s10853-011-5266-5

IIB 2010

Structures of a $\Sigma = 9$, [110]/{221} symmetrical tilt grain boundary in $SrTiO_3$

T. Mitsuma · T. Tohei · N. Shibata · T. Mizoguchi · T. Yamamoto · Y. Ikuhara

Received: 29 September 2010 / Accepted: 8 January 2011 / Published online: 25 January 2011

Abstract In this study, we fabricated a bicrystal of $SrTiO_3$ containing a $\Sigma = 9$, [110]/{221} symmetric tilt grain boundary (GB) and its atomistic structure was directly observed by transmission electron microscopy (TEM) and scanning TEM (STEM). We theoretically estimated the most stable structure by first principles calculations, and by combining this with TEM images determined the atomistic structure of the $\Sigma = 9$ grain boundary. We found that when the grain boundary is slightly tilted from the coincident site lattice (CSL) orientation, displacement shift complete (DSC) dislocations are introduced at the grain boundary to accommodate the misorientation between the two adjacent crystals while the most stable atomic structure remains unchanged.

Introduction

$SrTiO_3$ has recently attracted much attention because of its application in capacitors, thermistors [1], varistors [2], and as a substrate material. Since grain boundaries are important defect structures affecting the suitability of the material for these applications, many studies have been performed to understand their atomic-scale structures [3–8]. In general, a grain boundary can be defined as a function of five macroscopic geometrical degrees of freedom, and thus the properties of the grain boundary can be influenced by the misorientation angle between the two adjacent crystals. Bicrystal experiments have an advantage that the grain boundary structure can be arbitrary controlled, and are therefore ideal testing grounds to understand the relationship between the geometry and the properties of grain boundaries. There have been many studies on the atomistic structures of [001] tilt grain boundaries in $SrTiO_3$ [3–8], and the stable atomistic structures have been understood in detail from a view point of GB energy and the GB atomic configuration. However, there is little research on the DSC dislocations formed at these CSL grain boundaries.

In this study, a bicrystal of $SrTiO_3$ with a $\Sigma = 9$, [110]/{221} symmetric grain boundary was fabricated and used as a model system to clarify the relationship between atomistic configuration, GB energy, and DSC dislocations. The atomistic structure of the grain boundary was characterized by the combination of TEM and scanning TEM (STEM) imaging and first principles calculations. DSC dislocations are expected to be introduced to compensate the slight misorientation from the perfect $\Sigma = 9$ orientation.

Methods

Bicrystal fabrication and TEM observations

A $SrTiO_3$ bicrystal with a [110] symmetrical tilt grain boundary was fabricated by diffusion bonding of two single

T. Mitsuma · T. Tohei · N. Shibata · T. Mizoguchi · T. Yamamoto · Y. Ikuhara (✉)
Institute of Engineering Innovation School of Engineering, The University of Tokyo, 2-11-16, Yayoi, Bunkyo-ku, Tokyo 113-8656, Japan
e-mail: ikuhara@sigma.t.u-tokyo.ac.jp

T. Mitsuma
e-mail: mitsuma@sigma.t.u-tokyo.ac.jp

T. Yamamoto · Y. Ikuhara
Nanostructures Research Laboratory, Japan Fine Ceramics Center, Nagoya 456-8587, Japan

Y. Ikuhara
WPI Advanced Institute for Materials Research, Tohoku University, Sendai 980-8577, Japan

crystals. Figure 1 shows the schematic illustration of the bicrystal. The rotation axis is [110], and the grain boundary plane is set to be the {221} plane. To obtain the $\Sigma = 9$, [110]/{221} grain boundary orientation, 2θ is set to be 38.9°. The well-oriented bicrystals were joined and annealed in air at 1500 °C for 10 h. Specimens for TEM observation were then prepared following the standard TEM sample preparation procedure of mechanical grinding and ion thinning. TEM/STEM observations were conducted using conventional and high resolution TEM (JEM-2010HC operated at 200 kV and JEM-4010 operated at 400 kV), and aberration corrected STEM (JEM-2100F equipped with CEOS Cs corrector operated at 200 kV).

Calculation of grain boundary energy and structure

In order to examine stable structures and grain boundary energies theoretically, first principles calculations based on density functional theory have been performed to calculate grain boundary energies [9–18]. Recently, more precise methods to determine the atomistic structure of grain boundaries have been suggested (e.g., [19]), but in this study we assumed a stoichiometric grain boundary and calculated the most stable grain boundary structure. In order to determine the stable grain boundary structure, rigid body translations were considered. First, a supercell of the $\Sigma = 9$, [110]/{221} geometry was constructed, consisting of two grains. There is a grain boundary at both edges of each grain, giving a total of two grain boundaries in the supercell. We have used supercells as large as possible to try to minimize the interaction effect of these two grain boundaries. The relative translation between the two grains is not fixed in advance. It is then necessary to consider the rigid body translations when calculating the stable structure. The grain boundaries were made by rotating one grain by 19.47° and the other grain by −19.47° around the [110] axis to construct a $\Sigma = 9$, [110]/{221} grain boundary. The three mutually perpendicular directions defining the grain boundary supercell can be expressed in terms of the conventional cell for the lower grain in the supercell as follows: the x direction is along $[1\bar{1}4]$, the y direction is along $[2\bar{2}\bar{1}]$, and the z direction is along [110]. The lengths of each vector of the supercell are $X = 16.72$ Å, $Y = 25.65$ Å, and $Z = 5.575$ Å. The total number of atoms in the supercell is 180. After making the supercell, we took account of three dimensional rigid body translation (x, y, and z) of the grains with respect to each other. In this study, we performed calculations at translation intervals of 0.5 Å for all the dimensions. All atomic configurations in each supercell were then relaxed to obtain the most stable structure. In this study, the first principles projector augmented wave (PAW) method [16] within the generalized gradient approximation (GGA) [17] implemented in VASP code [18] was used. Wave functions were expanded in a plane wave basis set with a plane wave cutoff energy of 330 eV. In the calculation, a 2 × 1×3 k-point mesh was used. The optimized lattice constants in the present calculation were 3.942 Å which was consistent with the lattice constant of $SrTiO_3$.

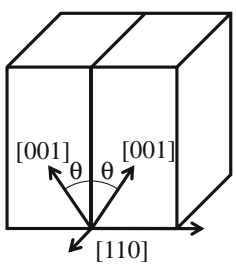

Fig. 1 Schematic illustration of the bicrystal fabricated in this study. ($\theta = 19.47°$)

Results and discussion

Figure 2 shows the TEM images of the $\Sigma = 9$, [110]/{221} grain boundary observed from the [110] direction; (a) shows the low magnification bright field (BF) TEM image; and (b) shows the electron diffraction pattern obtained from the grain boundary region. It is clear that there are no secondary phases such as amorphous phases in the grain boundary core, and the expected orientation relationship is successfully obtained. Figure 2c shows the HRTEM image of the grain boundary. From experimental HRTEM images and the corresponding electron diffractions patterns, we measured a misalignment of about 1° between the two $SrTiO_3$ crystals from the ideal $\Sigma = 9$ orientation. It is found that there are flat interface and step structures along the grain boundary. At the flat interface, the {221} plane is exactly the grain boundary plane. Because the flat interface constitutes a large fraction of the total interface structure, the flat structure should be the most stable structure of the given grain boundary orientation. The step structures are considered to be secondary defect structures of the grain boundary, compensating for the crystal misalignment. The steps have two kinds of structures, that is, up and down steps as shown in Fig. 2d. Both step structures consist of (111) and (001) planes. The step structures are periodically formed at about 20 nm intervals. The step height is about 5 Å.

First, the flat interface, which should be the most stable structure of the boundary, will be analyzed in detail. Figure 3 shows a high angle annular dark field (HAADF)-STEM image of the flat structure of the $\Sigma = 9$, [110]/{221} grain boundary. In HAADF STEM imaging, the intensity of the columns is roughly proportional to the square of the atomic number, Z [20]. In the present observation, the brightest spots correspond to the Sr–O

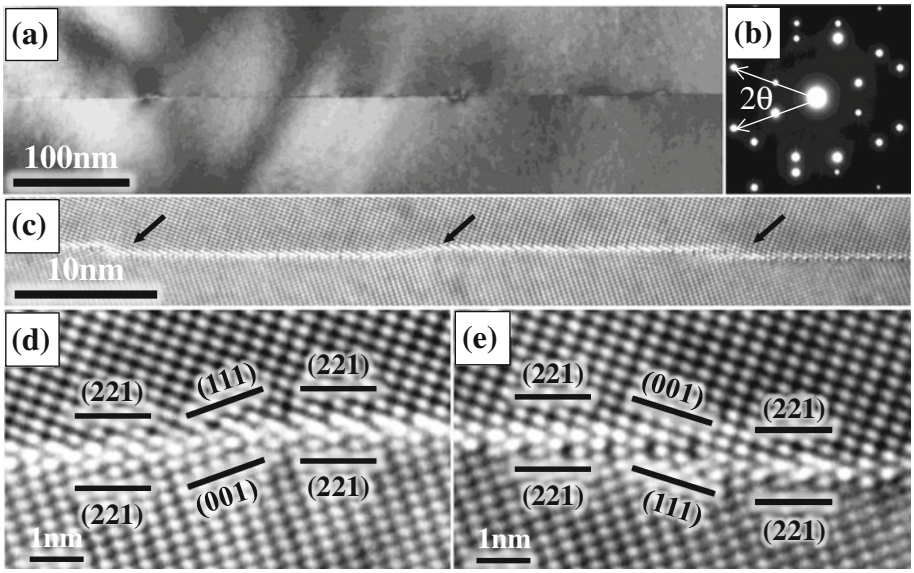

Fig. 2 **a** Low magnification BF TEM image of the $\Sigma = 9$, [110]/(221) grain boundary. **b** Diffraction pattern from the grain boundary. We succeeded in fabricating the grain boundary in the $\Sigma = 9$, [110]/(221) geometry and no secondary phase exists. **c** High resolution TEM image of the grain boundary. There are flat structures and step structures. Because the flat structure is longer, the flat structure must be the most stable structure at the grain boundary. At the flat structures, the (221) plane appeared. The step structures are secondary structure as indicated by *arrows*. **d**, **e** Two kinds of secondary structures, in which both step structures consist of (111) and (001) planes. The step structures appeared at 20 nm intervals

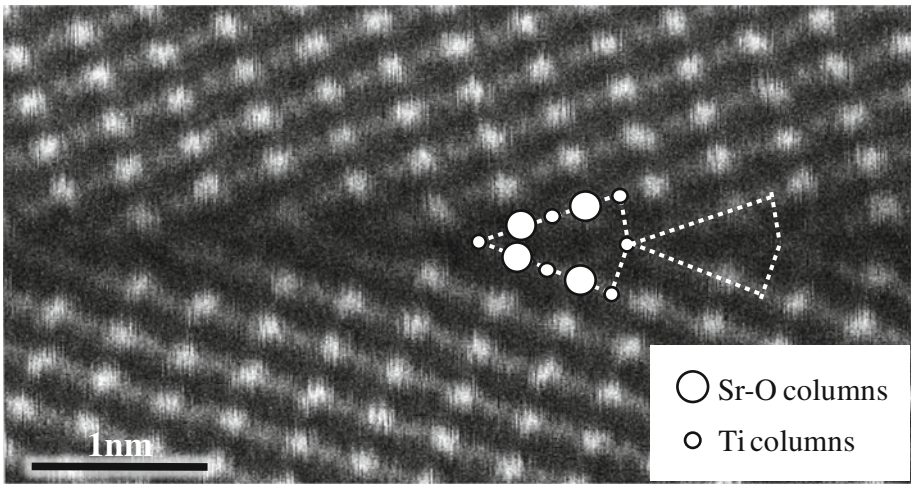

Fig. 3 HAADF STEM image of the $\Sigma = 9$, [110]/(221) grain boundary. The brightest spots are Sr–O columns, and the *less bright spots* are Ti columns, which are located in the repeated structural units

columns, and the less bright spots correspond to the Ti columns. Repeated structural units are observed at the grain boundary. The repeated structures are of quadrilateral shape, and Ti columns and O columns appeared at the interface. These structures are different from the bulk crystal structure.

Figure 4a shows a plot of calculated grain boundary energy vs. rigid body translation for the $\Sigma = 9$, [110]/{221} grain boundary. In the present calculation, we have used 180 atom supercells in order to minimize the boundary-boundary interaction in the repeated supercells. In the rigid body translation, we first considered translation along the *y* direction which, in our definition, corresponds to the separation between the two grains. We prepared supercells that are translated by 0.5 Å only along the *y* direction without making *z* and *x* translations. Structure optimization and total energy calculations were made for each *y* translation to find the equilibrium separation. We find the *y* translation with the lowest energy is 1 Å. After determining the separation along the *y* direction, we translated the structure along the *x* and *z* direction and relaxed each structure. In Fig. 4, we show calculated total energies for different translations along the *x* and *z* direction, with the *y* translation fixed at 1 Å. The figure shows that the GB energy depends on the rigid body translation. The most stable structure appears when the rigid body

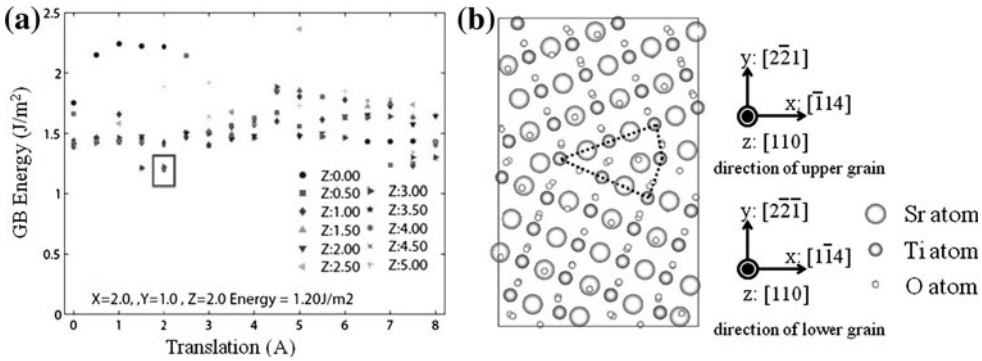

Fig. 4 **a** The results of calculations by VASP code. **b** The most stable structure by the calculation. The repeated structural units are consistent with those observed in the HAADF STEM image. At the termination plane, there are Ti columns and O columns

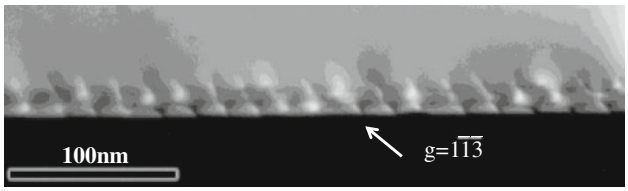

Fig. 5 Low magnification tilted *dark* field TEM image. Regularly aligned *bright line* contrast was observed. This contrast indicates DSC dislocations and appeared at 20 nm intervals

translation is at $x = 2.0$ Å, $y = 1.0$ Å, and $z = 2.0$ Å. Figure 4b shows the most stable grain boundary structure thus obtained for the $\Sigma = 9$, [110]/{221} grain boundary. The structure unit is quadrilateral in shape, and consists of Ti columns and Sr–O columns. Only Ti columns appear at the interface. Thus the most stable calculated grain boundary structure is consistent with the structure experimentally observed by HAADF STEM (Fig. 3). The flat interface is considered to be the most stable atomic structure at the $\Sigma = 9$, [110]/{221} grain boundary under the present fabrication conditions.

Next, we focus on the step structures. Figure 5 shows a low magnification dark field TEM image of the $\Sigma = 9$, [110]/(221) grain boundary. The grain boundary is slightly tilted from the viewing direction. There is periodic contrast along the grain boundary, and the interval of the periodic contrast corresponds well to that of the step structures observed in the HRTEM image. These contrast features are considered to correspond to the step structures. From this image, we assume that the step structures are related to the formation of DSC dislocations in order to accommodate the slight misorientation from the perfect $\Sigma = 9$ geometry. The termination plane does not change on either the right or the left side of the step structures as shown in Fig. 2. Therefore, the dislocations should be perfect dislocations. We can estimate the Burgers vector of the perfect dislocations at the grain boundary by CSL/DSC theory [21–28]. Let us therefore discuss the detail of CSL/DSC theory for $SrTiO_3$.

When the two misoriented single crystal structure models are overlapped, the coincidence site lattice appears. The CSL has three dimensional periodicities. Figure 6 shows the CSL plot of the $SrTiO_3$ $\Sigma = 9$, [110]/{221} grain boundary. Here, we only focus on the cation sites. Since oxygen sites form regular octahedra, the oxygen sites are regarded as sites with higher symmetry than the cation sites. Thus, we need to consider cation sites for discussing CSL and DSC theory. We label one crystal '*a*' and the other '*b*'. The cation sites labeled with '*a*' belong to crystal '*a*', and those labeled with '*b*' belong to crystal '*b*'. The indices '1' and '2' mean that the cation sites exist on different planes in depth along the [110] axis. The lattice represents the DSC lattice. The DSC lattice is defined as the coarsest lattice which covers all the cation sites. By the CSL/DSC theory, the Burgers vector of the perfect dislocations is a multiple of DSC lattice. When one crystal is moved along the Burgers vector of the perfect DSC dislocations, the same structure appears after the movement. In Fig. 6, the black arrows show the Burgers vectors of the perfect DSC dislocations. The upper arrow consists of $a/18$ [1$\bar{1}$4] and $a/2$ [110] components, and the lower arrow that is perpendicular to the grain boundary has an $a/9$ [2$\bar{2}\bar{1}$] component. Since the perfect DSC dislocations are introduced to accommodate the slight misorientation, the Burgers vector of the perfect dislocation has the edge component of $a/9$ [2$\bar{2}\bar{1}$] perpendicular to the grain boundary plane. This can be justified from the analysis based on the Frank's formula, from which we can calculate the misorientation from perfect sigma geometry.

$$D = \frac{|b_e|}{2\sin(\Delta\theta/2)} \approx \frac{|b_e|}{\Delta\theta} \quad (1)$$

The dislocation interval, D is estimated to be about 225 Å from the HRTEM image. The edge component of Burgers vectors of perfect dislocations is $a/9$ [2$\bar{2}\bar{1}$] and its absolute value is about 1.30 Å. We calculate the misorientation $\Delta\theta$ from the perfect $\Sigma = 9$ geometry as 0.96°. This result corresponds well to the angle deviation estimated from the experimental HRTEM image shown in Fig. 2. Thus, the step structure should be introduced in accordance with the perfect edge dislocations.

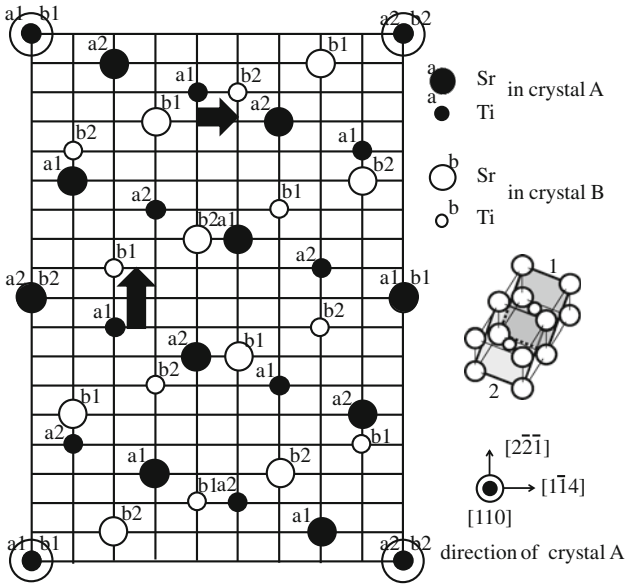

Fig. 6 The CSL/DSC lattice of cation sites of $SrTiO_3$. The *black circles* show the CSL. The indices '*a*' and '*b*' show the cation sites which are from crystals '*a*' and '*b*'. Cation sites can occupy different depths along the [110] direction and the indices 1 and 2 indicate cation sites that exist on the different depth plane. The black lattice shows the DSC lattice. The black arrows show the Burgers vector of perfect DSC dislocations

Next, the step height of the observed step structure will be further discussed. The step height can be also estimated from the CSL/DSC theory. When perfect dislocations are introduced along the grain boundary, the CSL moves and the same structure appears after the movement. In Fig. 7, after the movement, a new CSL appears at the position indicated by the double circle. We call the vector of the movement 'S1' or 'S2'. Figure 7 shows the vectors of movement of the CSL. 'S^{CL}' is the CSL length which is perpendicular (normal) to the grain boundary plane. The step height is '$S1_{edge}$', 'S^{CL}–$S1_{edge}$', '$2S^{CL}$–$S1_{edge}$', and so on. That is, the step heights are 'nS^{CL}–$S1_{edge}$' (n is an integral number). In the present case, the Burgers vector is $a/9$ [2$\bar{2}\bar{1}$], S^{CL} is a [2$\bar{2}\bar{1}$], $S1_{edge}$ is $5a/9$ [2$\bar{2}\bar{1}$]. The step height can be estimated as $5a/9$ [2$\bar{2}\bar{1}$], $4a/9$ [2$\bar{2}\bar{1}$], $13a/9$ [2$\bar{2}\bar{1}$], and so on. In other word, the step height is $(n-5/9)a$ [2$\bar{2}\bar{1}$]. Figure 8 shows one example of the formation of step structure in the case of $4a/9$ [2$\bar{2}\bar{1}$]. Figure 8a is a schematic illustration of the cation CSL/DSC plot of $SrTiO_3$. The larger circles are Sr sites, the smaller circles are Ti sites and the black circles are the CSL points. Figure 8b is the CSL/DSC plot after a movement by the Burgers vector of the perfect DSC dislocation. The Burgers vector of the perfect DSC dislocation is $a/9$ [2$\bar{2}\bar{1}$]. The step height is shown in this figure. In this case, the step height is $4a/9$ [2$\bar{2}\bar{1}$]. In experiments, from the HRTEM image, the step height is estimated to be about 5.2 Å, which corresponds to the value of $4a/9$ [2$\bar{2}\bar{1}$]. This fact again supports the notion that the step structures result from DSC dislocations

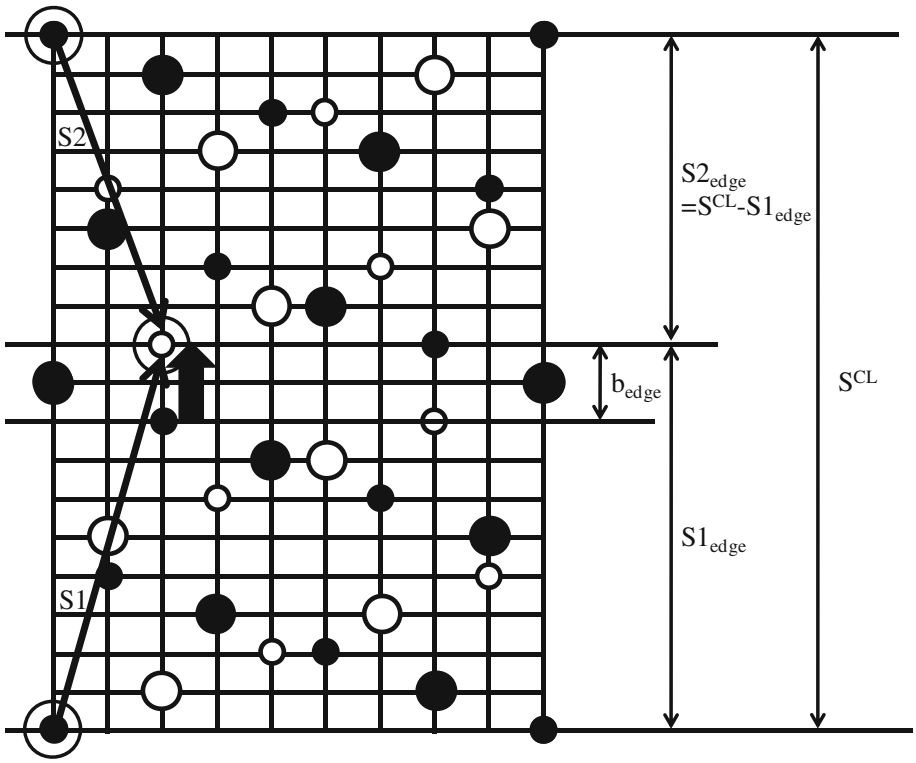

Fig. 7 The step height is determined by the CSL/DSC plot. When one crystal moved along the Burgers vector of the perfect dislocations, the CSL moved along the vector of S1 or S2. The step height is the edge component of S1 or S2

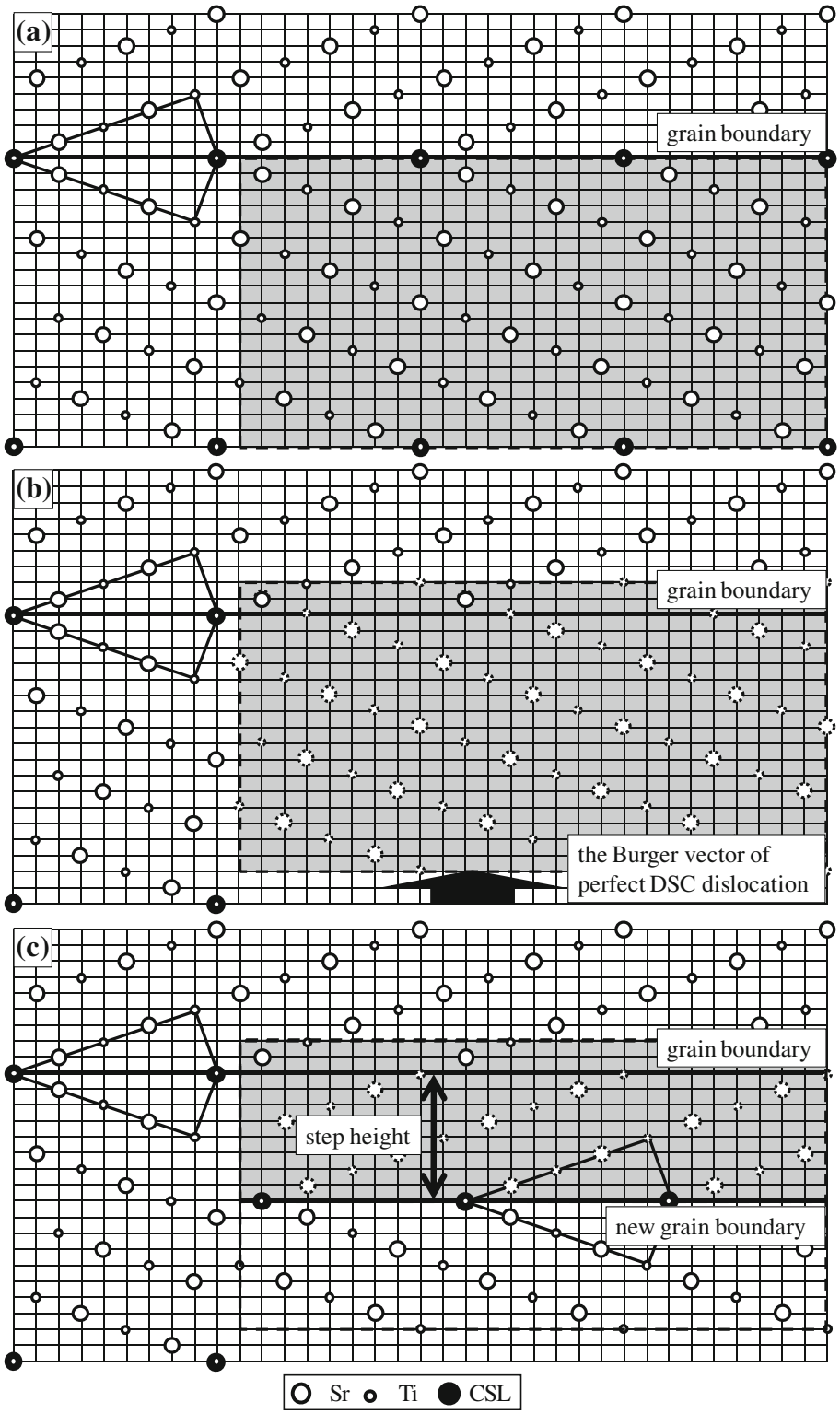

Fig. 8 An example of the formation of step structure. **a** Schematic illustration of the cation CSL/DSC plot of $SrTiO_3$. The *larger circles* are strontium sites, the *smaller circles* are titanium sites, and the *black circles* are CSL points. **b** After movement of the Burgers vector of perfect DSC dislocation. **c** After the lower grain moved. The grain boundary position has changed and the new CSL is evident at new grain boundary. The step height is shown in this figure

which are formed to accommodate the misorientation from the perfect $\Sigma = 9$ geometry.

Summary

In this study, we investigated the atomistic structure of the $\Sigma = 9$, [110]/{221} grain boundary by combining bicrystal experiments and theoretical calculations. The major results are summarized as follows:

- We directly observed the atomistic structure of the $\Sigma = 9$, [110]/{221} grain boundary. We found the structural units (repeated structure) along the grain boundary, which is different from the bulk structure. The structural unit consists of Sr–O columns and Ti columns. There are Ti columns and O columns at the interface.
- Grain boundary energy and stable structure was explored by first principles calculations. The theoretically obtained stable grain boundary structure well reproduces that observed in the HAADF STEM image.
- The observed periodic step-like structures at the present grain boundary were examined based on the CSL/DSC concept. The interval and step height of the step structure is well explained in terms of DSC theory, and it was concluded that the feature should be attributed to DSC dislocations that are introduced to accommodate small misorientation from the ideal $\Sigma = 9$ orientation.

Acknowledgements A part of this study was supported by Grant-in-Aid for Scientific Research on Priority Areas "Nano Materials Science for Atomic Scale Modification 474" and (A) 2224608 from Ministry of Education, Culture, Sports, Science and Technology (MEXT) of Japan.

References

1. Lewis GV, Catlow CRA, Casselton REW (1985) J Am Ceram Soc 68:555
2. Clarke DR (1999) J Am Ceram Soc 82:485
3. Mcgibbon MM, Browning ND, Chisholm MF, McGibbon AJ, Pennycook SJ, Ravikumar V, Dravid VP (1994) Science 266:102
4. Choi S-Y, Buban JP, Nishi M, Kageyama H, Shibata N, Yamamoto T, Kang S-JL, Ikuhara Y (2006) J Mater Sci 41:2621. doi:10.1007/s10853-005-2089-2
5. Kim M, Pennycook SJ (2000) Interface Sci 8:199
6. Zhang Z, Rühle M (2002) Phys Rev B 66:214112
7. Jia CL, Urban K (2004) Science 303:2001
8. Zhang Z, Rühle M (2003) Science 302:846
9. Imaeda M, Ikuhara Y (2008) Phys Rev B 78:245320
10. Nishimura H, Matsunaga K, Saito T, Yamamoto T, Ikuhara Y (2003) J Am Ceram Soc 86:574
11. Oba F, Tanaka I, Nishitani SR, Adachi H, Slater B, Gay DH (2000) Philos Mag A 80:1567
12. Sato Y, Mizoguchi T, Oba F, Ikuhara Y, Yamamoto T (2005) Phys Rev B 72:064109
13. Benedek NA, Finnis MW (2008) Phys Rev B 78:064110
14. Piskunov S, Borstel G (2004) Comput Mater Sci 29:165
15. Blochl PE (1994) Phys Rev B 50:17953
16. Jhon, Perdew P, Burke K, Ernzerhof M (1996) Phys Rev Lett 77:18
17. Kresse G, Furthmuller J (1996) Phys Rev B 54:11169
18. Liechtenstein AI, Anisimov VI, Zaanen J (1995) Phys Rev B 52:9
19. Alfthan S, Sutton AP (2010) Annu Rev Mater Sci 40:557
20. Pennycook SJ, Nellist PD (2000) Microsc Microanal 6:343
21. Bollmann W (1970) Crystal defects and crystalline interface. Springer-Verlag, New York
22. Bollmann W (1967) Philos Mag 16:363
23. Bollmann W (1967) Philos Mag 16:383
24. Shibata N, Ikuhara Y (2003) Philos Mag 83:2221
25. Balluffi RW, Brokman A, King AH (1982) Acta Metall 30:1453
26. Balluffi RW, Olson GB (1985) Metall Trans A 16A:529
27. Smith DA, Goodhew PJ (1982) Philos Mag A 46:161
28. Ishida Y, Mclean M (1972) Philos Mag 27:1125